

PACS numbers: 87.57.Ce; 87.64.Cc; 78.67.Bf
DOI: 10.1070/QE2007v037n01ABEH013461

Effect of multiple scattering of light by titanium dioxide nanoparticles implanted into a superficial skin layer on radiation transmission in different wavelength ranges

A.P. Popov, A.V. Priezzhev, J. Lademann, R. Myllylä

Abstract. **The propagation of radiation in different spectral ranges in a superficial skin layer partially filled with titanium dioxide nanoparticles at the volume concentration 0.67 % – 2.25 % is simulated by the Monte-Carlo method. This volume concentration corresponds to the maximum admissible concentrations of particles that most efficiently attenuate radiation in the independent scattering regime. The transmission of radiation at 307, 400, and 500 nm in a 20-μm thick skin layer is simulated and the effect of nanoparticles on the contributions from photons of different scattering orders to transmission is considered. It is shown that the administration of nanoparticles results in the broadening of the scattering-order distribution of photons propagated through the skin layer and the shift of the maximum of this distribution in the direction of a greater number of scattering events at wavelengths 400 and 500 nm, the effect being more pronounced at 400 nm. The increase in the scattering order elongates photon trajectories in the medium and enhances diffusely scattered radiation, thereby reducing transmission.**

Keywords: *propagation of optical radiation, nanoparticles, titanium dioxide, Monte-Carlo method, skin model.*

1. Introduction

The problem of protection of people from the harmful action of UV radiation, which can cause, for example, skin cancer is especially urgent at present due to the thinning of the ozone layer in the Earth atmosphere. The human skin is a protective barrier consisting of several layers [1]: the horny layer, epidermis, papillary derma, the upper plexus of blood vessels, reticular derma, the lower plexus of blood vessels, and subcutaneous fat. These layers have different scattering and absorption coefficients, refractive indices, and anisotropy scattering factor [2]. The layer located at the skin surface is called horny and consists of necrotic cells. This layer protects lower-lying layers against chemical, physical (in particular, optical), and other types of action. The horny layer prevents the penetration of UV radiation into epidermis and derma, which are located deeper in the skin. To increase the efficiency of this function, creams containing chemical (absorbing) and physical (absorbing and scattering) materials have been developed [3, 4]. The latter include titanium dioxide (TiO_2) and zinc oxide (ZnO) nanoparticles, which increase light reflection and absorption. The authors of [5] proposed to use silicon (Si) particles for this purpose.

The UV radiation spectrum is conventionally divided into three ranges [6]: UV-A (315 – 400 nm), UV-B (280 – 315 nm), and UV-C (100 – 280 nm). The short-wavelength part of UV radiation (UV-C), which is most hazardous for living organisms on Earth, is completely absorbed in the ozone layer located at a height of 18 – 40 km over the Earth surface, whereas the UV-A and UV-B radiation is absorbed only partially and their main part reaches the Earth surface [7]. The action of UV radiation on the human skin can be of two types: acute or chronic [8]. The first type includes the sun burn (caused by UV-B radiation) and tan (caused by UV-A radiation), as well as the synthesis of the D vitamin (caused by UV-B radiation), while the second one includes melanoma and photoaging caused by the action of UV-A radiation. Because of a decrease in the ozone layer thickness in recent years, the intensity of high-energy UV radiation penetrating into the lower layer of the atmosphere, which is the habitat of people, has become higher.

Nanoparticles are used in sunscreens to reduce UV-A and UV-B irradiation. TiO_2 particles absorb radiation at wavelengths $\lambda < 365$ nm, while ZnO particles absorb radiation at wavelengths $\lambda < 380$ nm. For this reason, the former are used to attenuate UV-B radiation and the short-wavelength part of UV-A radiation, while the latter are mainly used for protection from UV-A radiation [4]. The ability of TiO_2 to produce free radicals and singlet oxygen upon absorption of light in skin, which are hazardous for cells, are suppressed by using quartz (SiO_2) and corundum (Al_2O_3) coverings [9, 10]. The formation of aggregates and agglomerates of nanoparticles in creams results in the wavelength shift of radiation most efficiently interacting

A.P. Popov International Laser Center, M.V. Lomonosov Moscow State University, Vorob'evy gory, 119992 Moscow, Russia; present address: Department of Electrical Information Engineering, Optoelectronics and Measurement Techniques Laboratory, University of Oulu, P.O. Box 4500, 90014 University of Oulu, Finland; e-mail: dwelle@rambler.ru;
A.V. Priezzhev Department of Physics, International Laser Center, M.V. Lomonosov Moscow State University, Vorob'evy gory, 119992 Moscow, Russia; e-mail: avp2@phys.msu.ru;
J. Lademann Medical Faculty Charité, Center of Experimental and Applied Cutaneous Physiology, Humboldt University, Berlin, 10117, Germany; e-mail: juergen.lademann@charite.de;
R. Myllylä Department of Electrical Information Engineering, Optoelectronics and Measurement Techniques Laboratory, University of Oulu, P.O. Box 4500, 90014 University of Oulu, Finland;
e-mail: rist.myllyla@e.oulu.fi

Received 19 June 2006; revision received 7 November 2006
Kvantovaya Elektronika **37** (1) 17 – 21 (2007)
Translated by M.N. Sapozhnikov

with particles to the visible region and in the reduction of attenuation of UV radiation. New preparation techniques [4] make it possible to obtain small nanoparticles with a narrow size distribution (25 ± 4 nm), which are considerably less subjected to aggregation.

In this paper, we consider non-aggregating TiO_2 nanoparticles, which remain in the upper two-micron part of the 20-μm thick superficial skin layer upon applying a sunscreen cream on the skin. We studied the effect of such particles (of size 62, 122, and 176 nm) on the transmission of radiation at 307, 400, and 500 nm by the skin layer from the point of view of changes in the photon trajectories due the change in the order of their scattering by nanoparticles.

2. Experimental results

The distribution of TiO_2 particles over the horny layer depth was determined earlier in experiments by the stripping technique described in detail in [11, 12]. Here, we discuss this method only briefly. An emulsion containing TiO_2 particles of average diameter 100 nm was applied once per day on a skin area of size 10×8 cm on the inner side of a forearm and was rubbed in it. By the fourth day the horny layer was removed successively with the help of a medical scotch. The thickness of each strip of this layer near the skin surface was about 0.5 μm. As the depth of the horny layer from which skin strips were taken was increased, their thickness decreased due to a stronger adhesion between the cells of the layer (corneocytes) in the layer depth. The surface density of particles in strips determined from X-ray fluorescence measurements [13] was approximately 14 μg cm^{-2} in a strip taken from the skin surface and virtually zero in a strip taken from a depth of 20 μm. Nanoparticles were located predominantly at a depth of 0 – 3 μm. The experimental results are presented in Fig. 1 [14]. The volume concentration C of particles in a strip was estimated from the expression

$$C = \frac{NV_0}{V} = \frac{M}{\rho_0 V_0}\frac{V_0}{V} = \frac{M}{\rho_0 V}, \qquad (1)$$

where N is the number of particles in a strip of volume V; V_0 is the volume of a particle of density ρ_0; and M is the mass of all particles inside the strip. The volume V is equal to the product of the strip thickness (0.75 μm for the upper strip) by the surface area (1 cm^2). It follows from Fig. 1 that the mass M of the upper strip of area 1 cm^2 is 14 μg. The density of the rutile form of titanium dioxide is $\rho_0 = 4$ g cm^{-3}. Therefore, the concentration of particles in the upper strip is about 5 %. The concentration of particles in the horny layer parts located deeper is considerably lower.

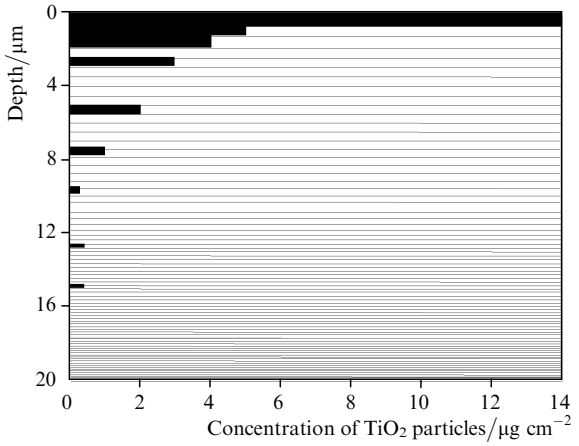

Figure 1. Distribution profile of titanium dioxide particles over the horny layer depth.

3. Calculations based on the Mie theory

We described the interaction of TiO_2 particles with radiation by using the Mie scattering theory because the shape of particles was assumed spherical, which is valid for particles of size more than 35 nm [15]. The calculation procedure is described in detail in our earlier paper [16]. The scattering (μ_s) and absorption (μ_a) coefficients for nanoparticles of diameter d at concentration C suspended in a transparent medium, which are required for Monte-Carlo simulations, are expressed in terms of the scattering (σ_s) and absorption (σ_a) cross sections of a nanoparticle (cross sections have the dimensionality of area). By using the same notation as in (1), we obtain

$$\mu_s = \frac{N\sigma_s}{V} = \frac{C}{V_0}Q_s\frac{\pi d^2}{4} = CQ_s\frac{\pi d^2/4}{\pi d^3/6} = 1.5\frac{Q_s C}{d}, \qquad (2)$$

$$\mu_a = \frac{N\sigma_a}{V} = \frac{C}{V_0}Q_a\frac{\pi d^2}{4} = CQ_a\frac{\pi d^2/4}{\pi d^3/6} = 1.5\frac{Q_a C}{d}, \qquad (3)$$

where $Q_s = \sigma_s/\sigma_g$ and $Q_a = \sigma_a/\sigma_g$ are the dimensionless factors of the scattering and absorption efficiency of a particle, respectively; and $\sigma_g = \pi d^2/4$ is the geometrical cross section of a spherical particle. The factors Q_s and Q_a are determined by using the Mie scattering theory implemented in the MieTab program 7.23 [17]. As the total value of coefficients ($\mu_s + \mu_a$) increases, the attenuation of radiation propagating through a layer of particles increases. Scattering by particles also depends on the anisotropy factor g (the average cosine of the scattering angle). Scattering by small particles is more isotropic than that by large particles, which reduces transmission. Thus, a combination of large scattering and absorption efficiency factors related to the particle diameter (which is proportional to μ_s and μ_a, respectively) and a small anisotropy factor enhances the attenuation of radiation.

The value of $[Q_s(1-g) + Q_a]/d$ was calculated for $\lambda =$ 307, 400, and 500 nm and particle diameters 35 – 200 nm (with a step of 2 nm). We used the refractive indices of the medium $n_m = 1.53$ [1] and nanoparticle material $n = 3.56 - i \times 1.72$ ($\lambda = 307$ nm), $3.13 - i \times 0.008$ ($\lambda = 400$ nm), and $2.82 - i \times 0.0$ ($\lambda = 500$ nm) [18]. The choice of the above wavelengths was not accidental: the first wavelength corresponds to the erythemal peak [14], the second one is located at the boundary of the UV and visible ranges, and the third one lies in the region of the maximum intensity of the solar spectrum. The results of calculations are presented in Fig. 2. One can see that the dependences have maxima. The most pronounced attenuation of radiation is observed for particles with diameters corresponding to the position of maxima of the curves. As shown earlier in [16], the most efficient in this sense for $\lambda = 307$ and 400 nm are particles with diameters 62 and 122 nm, respectively. For $\lambda = 500$ nm, as follows from

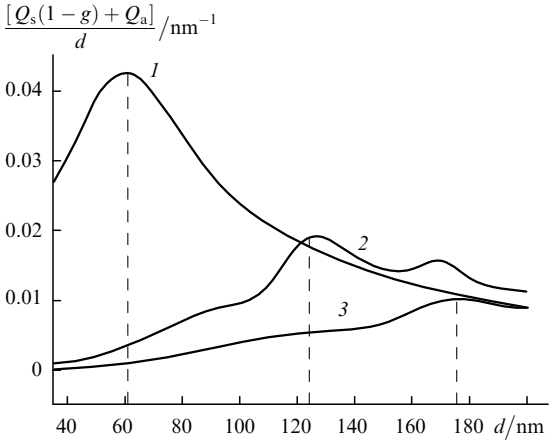

Figure 2. Dependences of the quantity $[Q_s(1-g)+Q_a]/d$ on the TiO_2 particle diameter for radiation at 307 (*1*), 400 (*2*), and 500 nm (*3*) calculated by using the Mie theory. The vertical dashed straight lines correspond to the optimal diameters of particles.

calculations, attenuation occurs most efficiently when particles of diameter 176 nm are used.

4. Monte-Carlo simulations

The propagation of radiation in a horny layer with TiO_2 particles was simulated by the Monte-Carlo method by using the computer program described in our papers [14, 16, 19]. The model of the horny layer is shown in Fig. 3. The layer is represented by two plane infinitely broad layers without a distinct interface: the upper 2-μm thick layer containing TiO_2 particles and the lower layer without particles. The total thickness of both layers is 20 μm, which corresponds to the horny layer on a greater part of the human body surface [20]. We assume that the sample borders the air on one side and epidermis with the refractive index 1.5 on another. The number of photons injected into skin was 1 million in each calculation. The results of calculations are normalised to this value. The use of such a number of photons gives the acceptable calculation time (about 5 min for each set of parameters) and provides the statistical error less than 3 %. The program was used to calculate the number of photons absorbed in the upper (with particles) and lower (without particles) parts of the horny layer, as well as the number of photons propagated through the entire horny layer and diffusely reflected from it (detected on the skin surface).

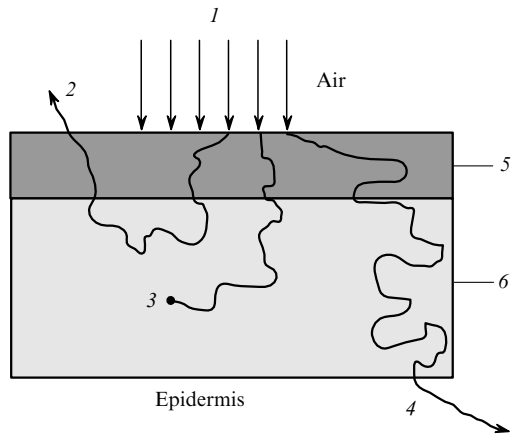

Figure 3. Model of the horny layer partially filled with TiO_2 particles used in Monte-Carlo simulations: (*1*) incident radiation; (*2*) diffusely reflected radiation; (*3*) absorbed radiation; (*4*) transmitted radiation; (*5*) 2-μm thick upper part of the horny layer (with TiO_2 particles); (*6*) lower part of the horny layer (without TiO_2 particles). The thickness of the entire horny layer [(*5*) and (*6*)] is 20 μm.

Scattering in the upper part of the horny layer was simulated by using the hybrid phase function representing a linear combination of phase Mie functions (scattering by spherical particles) and Henyey – Greenstein functions (scattering in biological tissues):

$$p(\theta) = 2\pi A p_{\mathrm{Mie}}(\theta) + (1-A)p_{\mathrm{HG}}(\theta), \tag{4}$$

$$p_{\mathrm{HG}}(\theta) = \frac{1}{2}\frac{1-g^2}{(1+g^2-2g\cos\theta)^{3/2}}, \tag{5}$$

$$\int_0^{\pi} p(\theta)\sin\theta\,\mathrm{d}\theta = 1, \tag{6}$$

where $A = \mu_s^{(1)}/(\mu_s^{(1)}+\mu_s^{(2)})$; $\mu_s^{(1)}$ is the scattering coefficient of TiO_2 particles at concentration C suspended in a transparent medium, determined from (2); $\mu_s^{(2)}$ is the scattering coefficient of the horny layer; and θ is the scattering angle. Table 1 presents the optical properties of the horny layer without and with particles for the radiation wavelengths used in simulations. The concentration of TiO_2 particles was 0.67 %, 1.70 %, and 2.25 % for radiation at wavelengths 307, 400, and 500 nm, respectively. These are maximum admissible particle concentrations at which the scattering of radiation by particles is independent of the presence of other particles (independent scattering). It is assumed that such scattering occurs when the distance between surfaces of particles is not smaller than the radiation wavelength in the medium [22]. If we assume that spherical particles are located inside imaginary cubes in the medium, the expression relating the critical concentration C_{cr} of particles with the particle diameter d has the form

$$\frac{\pi d^3/6}{(d+\lambda/n_{\mathrm{m}})^3} = C_{\mathrm{cr}}, \tag{7}$$

where λ/n_{m} is the radiation wavelength in the medium. The ratio of particle and cube volumes in the left-hand side of

Table 1. Optical parameters of the upper part of the horny layer in the absence and presence of particles in it, and the refractive index of TiO_2 particles.

λ/nm	Horny layer without TiO_2 particles [21]				Horny layer with TiO_2 particles				
	μ_s/mm^{-1}	μ_a/mm^{-1}	g	n_{m}	d/ nm	C_{cr} (%)	μ_s/mm^{-1}	μ_a/mm^{-1}	n [18]
307	240	60			62	0.67	426	337	$3.56 - i \times 1.720$
400	200	23	0.9	1.53	122	1.70	1106	37	$3.13 - i \times 0.008$
500	162	7			176	2.25	845	7	$2.82 - i \times 0.000$

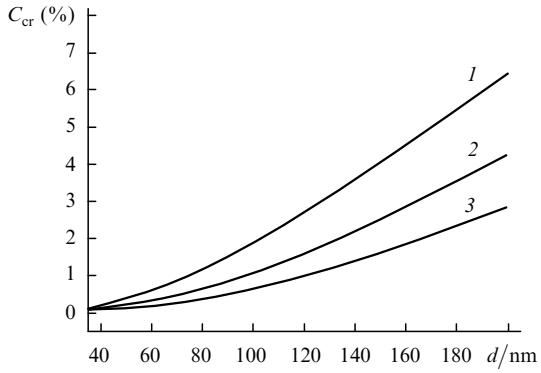

Figure 4. Dependences of the critical volume concentration of spherical nanoparticles on their diameter for radiation at 307 (*1*), 400 (*2*), and 500 nm (*3*).

(7) gives the critical volume concentration. The dependence $C_{cr}(d)$ is shown in Fig. 4.

5. Simulation results and discussion

Figure 5 presents the distribution diagrams for the number of photons at 307, 400, and 500 nm absorbed in the upper (with TiO_2 particles) and lower (without particles) parts of the horny layer and reflected from this layer and transmitted through it. One can see that the presence of particles in the upper two-micron part of the horny layer differently affects the attenuation of transmitted radiation. For the radiation wavelength of 307 nm, attenuation is mainly caused by the increase in the total absorption (due to increasing absorption in the upper part of the layer containing particles) from 75 % to 85 %. For wavelengths 400 and 500 nm, the situation is different: attenuation mainly occurs due to increasing reflection (diffuse and surface). Thus, the total absorption at 400 nm increases from 45 % to 51 %, while reflection increases from 6 % to 19 %. Absorption at 500 nm increases from 17% to 21% and reflection – from 6.5 % to 18 %. The difference in the attenuation mechanisms is explained by the properties of the particle material in which radiation with $\lambda < 365$ nm is absorbed and scattered, whereas longer-wavelength radiation is only scattered. Despite this, absorption in the part of the horny layer with particles also increases at 400 and 500 nm, which is caused by the bending and elongation of photon trajectories in this part of the horny layer containing particles.

The effect of TiO_2 particles on the number of scattering events experienced by photons migrating in the horny layer is illustrated in Fig. 6. The distributions over scattering orders of photons transmitted through the entire layer (to epidermis) are presented for radiation wavelengths used in simulations in the cases when the upper part of the horny layer does not contain particles or contains particles of a certain size and concentration. The curves in Fig. 6a virtually coincide, which means that absorption dominates

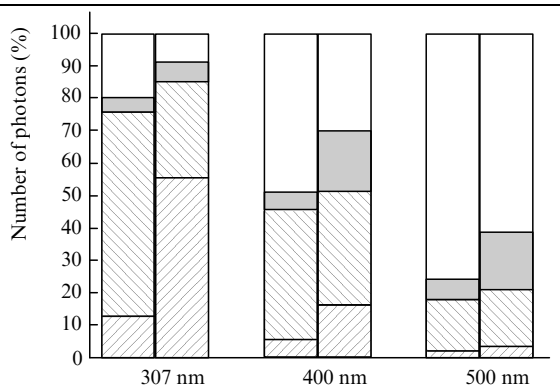

Figure 5. Distribution diagrams of photons over the following groups (from bottom to top): photons absorbed in the upper part of the horny layer (with TiO_2 particles), absorbed in the lower part of the layer (without particles), reflected from this layer (diffusely and from the layer–air interface) and transmitted through the entire layer, for $\lambda = 307$ nm ($d = 62$ nm, $C = 0.62$ %), $\lambda = 400$ nm ($d = 122$ nm, $C = 1.70$ %), and $\lambda = 500$ nm ($d = 176$ nm, $C = 2.25$ %). The diagram at the left for each of the wavelengths corresponds to the zero concentration of particles.

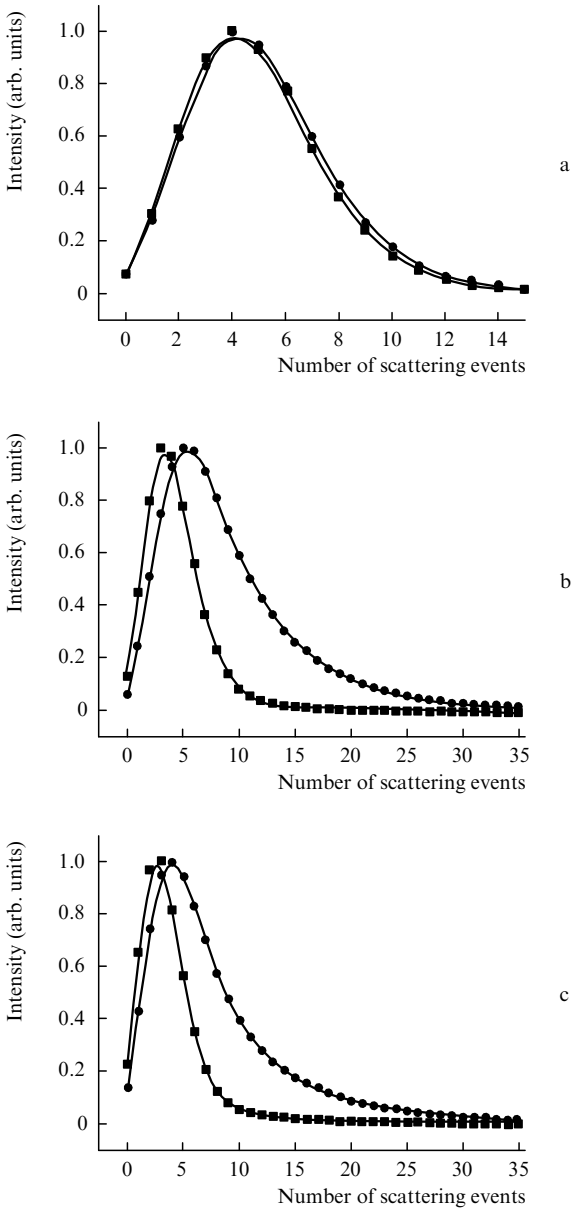

Figure 6. Scattering-order distributions of photons propagated through the entire horny layer in the absence (■) and presence (●) of particles in the upper part of the layer for $\lambda = 307$ nm, $d = 62$ nm, $C = 0.62$ % (a), $\lambda = 400$ nm, $d = 122$ nm, $C = 1.70$ % (b), and $\lambda = 500$ nm, $d = 176$ nm, $C = 2.25$ % (c).

over scattering. The corresponding curves in Figs 6b and 6c differ from each other: the introduction of particles leads to the increase in the distribution width and the shift of the distribution maximum in direction of a greater number of scattering events. Thus, the FWHM of the distribution changes from 5 to 10 and from 5 to 7 for $\lambda = 400$ and 500 nm, respectively, while the distribution maximum shifts from 3 to 5 and from 3 to 4 for the same wavelengths. A weaker effect for $\lambda = 500$ nm and particles of diameter 176 nm is caused by the lower values of the product of $[Q_s(1-g) + Q_a]/d$ by the volume concentration of particles (see Figs 2 and 4) compared to those for $\lambda = 400$ nm and particles of diameter 122 nm: 22.5×10^{-5} nm^{-1} ($C = 0.0225$) versus $C = 34 \times 10^{-5}$ nm^{-1} ($C = 0.017$).

6. Conclusions

We have studied the effect of titanium dioxide particles on the attenuation of radiation in the superficial (horny) layer of human skin at wavelengths of 307, 400, and 500 nm. The investigation has been performed by using calculations based on the Mie scattering theory and subsequent Monte-Carlo simulations. The results have shown that the scattering-order distribution of photons at 307 nm transmitted through the horny layer almost does not change after the implantation of nanoparticles ($d = 62$ nm, $C = 0.67$ %) because absorption of photons in these particles dominates. For radiation at 400 and 500 nm, the effect of particles ($d = 122$ nm, $C = 1.7$ % and $d = 176$ nm, $C = 2.25$ %, respectively) on scattering in the independent scattering regime is pronounced: the maximum of the scattering-order distribution shifts from 3 to 5 and from 3 to 4 scattering events, while its width is doubled and increases by a factor 1.4, respectively. This results in the elongation of photon trajectories and the increase in diffusely reflected radiation, thereby reducing transmission.

Acknowledgements. A.P. Popov thanks the Infotech Graduate School for financial support.

References

1. Tuchin V.V. *Tissue Optics* (Bellingham: SPIE Press, 2000).
2. Tuchin V.V. *Handbook of Optical Biomedical Diagnostics* (Bellingham: SPIE Press, 2002).
3. Edlich R.F., Winter K.L., Lim H.W., Cox M.J., Becker D.G., Horovitz J.H., Nichter L.S., Britt L.D., Long W.B. *J. Long-Term Effects Med. Implants*, **14**, 317 (2004).
4. Innes B., Tsuzuki T., Dawkins H., Dunlop J., Trotter G., Nearn M.R., McCormick P.G. *Cosmetics, Aerosols and Toiletries in Australia*, **15** (10), 21 (2002).
5. Rybaltovskii A.O., Bagratashvili V.N., Belogorokhov A.I., Koltashev V.V., Plotnichenko V.G., Popov A.P., Priezzhev A.V., Ishchenko A.A., Sviridova A.A., Zaitseva K.V., Tutorskii I.A. *Opt. Spektrosk.*, **101**, 626 (2006).
6. McKinlay A.F., Diffey B.L. *CIE J.*, **6**, 17 (1987).
7. Diffey B.L. *Phys. Med. Biol.*, **36**, 299 (1991).
8. Diffey B. *Phys. Med. Biol.*, **49**, R1 (2004).
9. Warner W.G., Yin J.J., Wei R.R. *Free Rad. Biol. Med.*, **23**, 851 (1997).
10. Lademann J., Weigmann H.-J., Schaefer H., Mueller G., Sterry W. *Skin Pharmacol. Appl. Skin Physiol.*, **13**, 258 (2000).
11. Weigmann H., Lademann J., Meffert H., Schaefer H., Sterry W. *Skin Pharmacol. Appl. Skin Physiol.*, **12**, 34 (1999).
12. Jacobi U., Meykadeh N., Sterry W., Lademann J. *J. Dt. Dermatol. Gesell.*, **1**, 884 (2003).
13. Lademann J., Weigmann H.-J., Rickmeyer C., Barthelmes H., Schaefer H., Mueller G., Sterry W. *Skin Pharmacol. Appl. Skin Physiol.*, **12**, 247 (1999).
14. Popov A.P., Priezzhev A.V., Lademann J., Myllylä R. *J. Phys. D: Appl. Phys.*, **38**, 2564 (2005).
15. Shao Y., Schlossman D. *Proc. Personal Care Ingredients Asia Conf.* (Shanghai, 1999) pp 1 – 9.
16. Popov A.P., Lademann J., Priezzhev A.V., Myllylä R. *J. Biomed. Opt.*, **10**, 064037 (2005).
17. http://pauli.nmsu.edu/~amiller/.
18. Ribarsky M.W., in *Handbook of Optical Constants of Solids*. Ed. by E.D. Palik (Orlando: Acad. Press, 1985).
19. Popov A.P., Priezzhev A.V., Lademann J., Myllylä R. *Opt. Zh.*, **73**, 67 (2006).
20. Sinichkin Yu.P., Utts S.R. *In vivo otrazhatel'naya i fluorestsentnaya spektroskopiya kozhi cheloveka* (In vivo Reflection and Fluorescence Spectroscopy of the Human Skin) (Saratov: Saratov State University, 2001).
21. Tuchin V.V. *Lazery i volokonnya optika v biomeditsinskikh issledovaniyakh* (Lasers and Fibre Optics in Biomedical Studies) (Saratov: Saratov State University, 1998).
22. McNeil L.E., French R.H. *Acta Mater.*, **48**, 4571 (2000).